DFT and Experimental Examination of the Oxidation/Reduction of a Thiol-Substituted Carotenoid with Gold versus Glassy Carbon Electrodes

Yunlong Gao,[†] A. Ligia Focsan,[‡] Yuan Yuan Li,[†] and Lowell D. Kispert*[,‡]

Key Lab of Analytical Chemistry for Life Science, School of Chemistry and Chemical Engineering, Nanjing University, Nanjing, 210093, P R China, and Department of Chemistry, Box 870336, University of Alabama, Tuscaloosa, Alabama 35487-0336

Received: April 14, 2006; In Final Form: June 22, 2006

The oxidation/reduction properties of the thiol-substituted carotenoid, 7′-apo-7′-(4-mercaptomethylphenyl)-β-carotene (AMC), on gold and glassy carbon electrodes were investigated. Similarities of the first and second oxidation potentials of AMC when the glassy carbon electrode is used are attributed to stabilization of the dication in the presence of CH_2Cl_2. This does not occur for AMC tethered to gold, where the second oxidation potential is higher than the first by 145 mV. Self-assembled monolayers between AMC and the gold electrode causes the first oxidation potential to be lower by 90 mV than that on glassy carbon electrode. These phenomena are examined with density functional theory (DFT) calculations, which show that the ionization potential for the AMC−transition metal complex is lower than that of AMC. DFT calculations also show that the LUMO of the carotenoid−transition metal complex is independent of the chain length of the carotenoid but is related to the transition metal. Upon reduction at −1.185 V versus SCE the C−S bond of self-assembled AMC is cleaved.

Introduction

Extensive electrochemical studies[1] using platinum electrodes, confirmed by density functional (B3LYP) quantum chemical calculations, revealed the inversion of the standard potentials of the first and second electron transfers in the oxidation of β-carotene and 15,15′-didehydro-β-carotene (but not in their reduction) as well as in the reduction of canthaxanthin (but not in its oxidation). Two main interconnected effects were deduced. One is the localization of the charges of the di-ion toward the ends of the long conjugated molecule at a large distance from one another, thus minimizing Coulombic repulsions. The localization of charges also favors solvation of the di-ion giving rise to additional stabilization. The charge in the ion radical is delocalized over the entire polyene chain, which disfavors stabilization by interaction with the solvent. These two solvation effects allow for potential inversion by 30 mV, which cannot occur if the two electrophores are linked by a saturated bridge.[1] Localization of the charges in the di-ion is favored by the presence of electron-accepting terminal groups of reduction (carbonyl groups in canthaxanthin) and hole-accepting groups for oxidation of β-carotene.

In this paper, we examine the standard oxidation potentials of the first and second electron transfers of a carotenoid tethered to an electrode at one end of the conjugated chain, thus reducing the effect of solvation at both ends of the carotenoid. Such a study is possible with a thiol-substituted carotenoid, 7′-apo-7′-(4-mercaptomethylphenyl)-β-carotene (AMC), which can form self-assembled on monolayers (SAMs) gold surfaces.[2] The electrochemical behavior of a carotenoid self-assembled on gold can be compared to that when using a glassy carbon electrode, where no self-assembly can occur and thus the carotenoid dication can be additionally stabilized by the solvent.

CHART 1

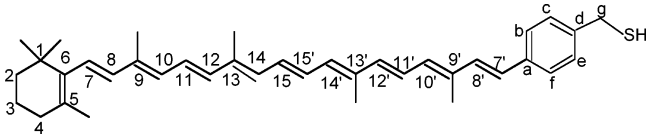

Saturated organosulfur compounds such as alkanethiolates are known to form self-assembled monolayers on metal surfaces,[3] and various features of SAM's have been reviewed extensively.[4−8] The properties of electroactive SAMs have attracted considerable interest because of their potential application in molecular devices.[9] Molecules that contain a long conjugated system, such as carotenoid derivatives,[2] phenylene-vinylene,[10] and phenyleneethynylene[11] and others,[12,13] have been synthesized and also incorporated into SAMs. Of these molecules, carotenoid polyenes appear to be excellent candidates for molecular wires because of their conjugated nature and the planar conformation of the alkene chain, which maximizes overlap of the π electrons. Despite the demonstration of promising molecular-electronic devices,[14−17] the nature of the junction between molecules and metals is still unclear.[18] Previous studies[19,20] have shown that the conductivity of *n*-alkenes is enhanced enormously when metal "contact pads" are covalently bonded to each end of the molecule and a conducting atomic force microscope probe is used to contact the top metal surface (a gold nanoparticle).

Recently, a thiol-substituted carotenoid, 7′-apo-7′-(4-mercaptomethylphenyl)-β-carotene (AMC) (Chart 1), was synthesized.[2] This material is over one million times more conductive than long-chain alkanethiols, suggesting that the carotenoid acts as a molecular wire.[2] Infrared and UV−vis spectroscopy, contact

* Corresponding author. E-mail: lkispert@bama.ua.edu.
[†] Nanjing University.
[‡] University of Alabama.

10.1021/jp0623239 CCC: $33.50
Published on Web 08/02/2006

angle measurements, ellipsometry, and XPS (X-ray photoelectron spectroscopy) data indicate that AMC molecules self-assemble on gold surfaces.[21] The monolayers are less ordered than alkanethiols because of steric hindrance along the polyene backbone and the bulky terminal β-ionone group. Nevertheless, they still form a hydrophobic interface. The polymer chains are disordered, and XPS spectra suggest that AMC molecules absorb on Au surfaces as thiolates.

In this study, we investigated the electrochemistry of AMC on gold and glassy carbon electrodes with the aim of ascertaining how chemisorption of AMC affects the electron transfer between AMC and the gold electrode. Because AMC is chemisorbed on the gold surface, solvation of the AMC radical cation, dication, radical anion, and dianion should be altered, and thus the difference between the first and second oxidation potentials and that between the first and second reduction potentials on a gold should be different from those on a glassy carbon electrode. Density functional quantum chemistry calculations (DFT) were carried out to examine the ground-state energies and the oxidation potential of the AMC−transition metal complex as well as the dependence on chain length of the carotenoids.

Experimental Section

Chemicals. 7′-apo-7′-(4-mercaptomethylphenyl)-β-carotene (AMC) was a gift from Devens Gust's group (Department of Chemistry and Biochemistry, Arizona State University). Anhydrous dichloromethane (CH_2Cl_2) was purchased from Aldrich. Tetrabutylammonium hexafluorophosphate (TBAHFP) was obtained from Fluka.

Electrochemistry. Cyclic votammetry (CV) and Osteryoung square-wave voltammetry (OSWV) measurements were performed by using a BAS-100 B/W electrochemical analyzer in a conventional three-electrode system at room temperature. TBAHFP was the supporting electrolyte. Gold and glassy carbon disks (diameter for gold electrode is 1.6 mm and that for glassy carbon is 3 mm) were used as working electrodes, a platinum wire was used as the auxiliary electrode, and a saturated calomel electrode (SCE) was used as the reference electrode. The working electrodes were prepared with the polishing tool supplied by BAS before each experiment. AMC CH_2Cl_2 solution was prepared in a N_2 drybox. The concentration of AMC is 1 mM, and that of TBAHFP is 0.1 M. The DigiSim CV simulation program (version 2.0), written by Rudolph et al.,[22] was supplied by BAS.

DFT Calculations. Functional B3LYP[23] included in the *Gaussian 03* package[24] was used in the DFT calculations.

Results and Discussion

Cyclic voltammetry of the electrochemical oxidation−reduction cycle of carotenoids (Car) in CH_2Cl_2 has been well studied, and several electrode and homogeneous reactions (Scheme 1) have been identified.[25−33] Typically,[33] the oxidation−reduction CV for a carotenoid such as canthaxanthin consists of five peaks. Peak 1 is due to the formation of the radical cation (eq 1). Peak 2 at a slightly higher oxidation potential is due to the formation of the carotenoid dication by a one electron oxidation of the radical cation (eq 2). Peaks 3 and 4 are the subsequent one-electron reductions of the dication and the radical cation, respectively (reverse of eqs 1 and 2). Peak 5 is due to the formation of the neutral carotenoid radical formed by the loss of H+ from the 5 or 5′ (or possibly 9′ or 9, or 13′ or 13) methyl group of the dication (eqs 6 and 3) followed by reduction. EPR studies[26,29] and electrochemical simulations have established the equilibrium given by eq 4. Electrochemical-EPR studies confirmed[29] the existence of the equilibrium (eq 4) by the reappearance of the radical cation EPR signals following the electron transfer between diffusing excess carotenoid and the dication after the diamagnetic dication is formed by extensive electrolysis. The equilibrium constant (K) for eq 4 varies over approximately 4 orders of magnitude, being the largest ($K \approx 10^3$) for carotenoids with high oxidation potentials, such as those with electron acceptor groups like canthaxanthin (keto group) or dicyano groups to the lowest ($K \approx 1$) for those carotenoids with donor groups like β-carotene, which exhibits some of the lowest oxidation potentials measured to date.

SCHEME 1

Electrode reactions:

$$\mathrm{Car} \rightleftharpoons \mathrm{Car}^{\bullet+} + e^- \quad (1)$$

$$\mathrm{Car}^{\bullet+} \rightleftharpoons \mathrm{Car}^{2+} + e^- \quad (2)$$

$$\#\mathrm{Car}^{\bullet} \rightleftharpoons \#\mathrm{Car}^{+} + e^- \quad (3)$$

Homogeneous reactions:

$$\mathrm{Car}^{2+} + \mathrm{Car} \rightleftharpoons 2\mathrm{Car}^{\bullet+} \quad (4)$$

$$\mathrm{Car}^{2+} \rightleftharpoons \#\mathrm{Car}^{+} + H^+ \quad (5)$$

$$\mathrm{Car}^{\bullet+} \rightleftharpoons \#\mathrm{Car}^{\bullet} + H^+ \quad (6)$$

#Car represents the carotenoid with one less proton

The CV was recorded (Figure 1a) after the gold electrode had been immersed in the AMC CH_2Cl_2 solution until AMC SAM formation had taken place.[21] Peaks 1 and 2 are oxidation peaks of Car and $Car^{\bullet+}$, respectively; peaks 3, 4, and 5 are reduction peaks of Car^{2+}, $Car^{\bullet+}$, and $\#Car^{+}$, respectively. The peak-to-peak separation for the first redox pair is only 42 mV at scan rate 1000 mV/s, indicating that the electron transfer between AMC and the gold electrode is very fast, in accord with chemisorption and SAM formation on the gold electrode. The appearance of peak 5 confirms the formation of Car^{2+} from which $\#Car^{+}$ is produced.[25−33] Because the DigiSim CV simulation program cannot be used to simulate a CV process that is not diffusion-controlled, the electron-transfer rate constants and redox potentials cannot be obtained by simulation. The redox potentials listed in Table 1 for the first and second electron transfers are averages of the observed oxidation and reduction peak potentials. The second oxidation potential is higher than the first by 145 mV; the same as observed[33] for 8′-Apo-β-carotenal in CH_2Cl_2 solution using a Pt electrode.

Figure 1b shows the oxidation CV and DigiSim simulation CV of AMC on a glassy carbon electrode at a scan rate of 500 mV/s. Soaking the electrode in the AMC CH_2Cl_2 solution for 30 min prior to measurement had no effect on the CV. The presence of the reduction peak of $\#Car^{+}$ (peak 5) indicates that two electrons can be transferred in the oxidation. Thus, the broad peaks are due to overlap of the two oxidation and two reduction peaks. The first and second oxidation peaks cannot be separated by high-resolution OSWV measurements. Best-fit DigiSim simulation (Figure 1b, Table 1) is obtained when the two oxidation potentials are very similar. It should be noted that the first oxidation potential on the gold electrode is lower than that on the glassy carbon electrode by about 100 mV. To investigate the similarity of oxidation potentials in this case, the charge distributions in the AMC radical cation ($AMC^{\bullet+}$) and dication (AMC^{2+}) were calculated by B3LYP/G-31G(d,p).

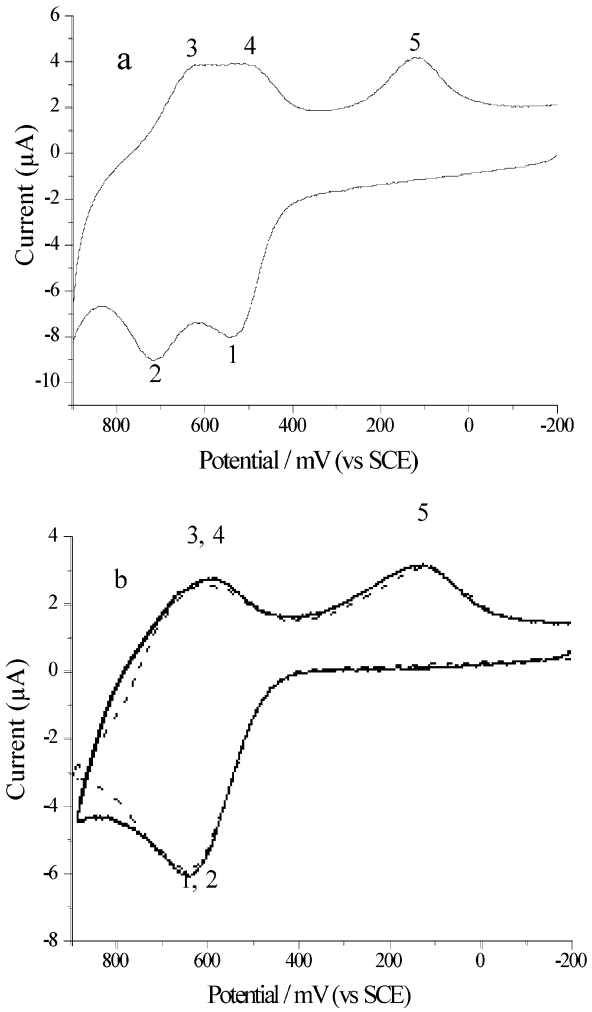

Figure 1. (a) Oxidation−reduction CV of AMC on a gold electrode. Scan rate: 1000 mV/s. (b) Experimental (solid line) and simulation (dashed line) of oxidation−reduction CV of AMC on a glassy carbon electrode. Scan rate: 500 mV/s.

TABLE 1: First and Second Oxidation Potentials (vs SCE) of AMC on Gold and Glassy Carbon Electrodes, and the Reduction Potentials (vs SCE) of AMC on Gold and Glassy Carbon Electrodes

electrode	oxidation potentials (mV) ±5		reduction potentials (mV) ±5	
	first	second	first	second
gold	520	665	−1800[a]	−1800[a]
glassy carbon	612	616	−1604	−1670

[a] Reduction potentials of desorbed AMC−Au after rupture of a C−S bond and in the presence of adsorbed S. Apparent reductive desorption occurred at −1185 mV.

The structure of AMC was built based on the reported X-ray structure[34] of β-carotene. In the optimized geometry, calculated by B3LYP/G-31G(d,p), the benzene ring, the C_d−Cg bond, and the chain are in the same plane. The C_d−Cg−S angle is 107.6°, and the Cg−S−H angle is 98.7°. The calculated excess charge differences (DD_{excess}) between $AMC^{\bullet+}$ and AMC and those between AMC^{2+} and AMC are shown in Figure 2a and b, respectively. Note, the *y*-axis scale in Figure 2b is twice that of Figure 2a. For brevity, the charges at the benzene ring and Cg are added together as T and the charges at adjacent carbon atoms in the conjugated chain are added together. In $AMC^{\bullet+}$, the positive charge is distributed over the conjugated chain. In AMC^{2+}, the positive charge distribution exhibits two maxima,

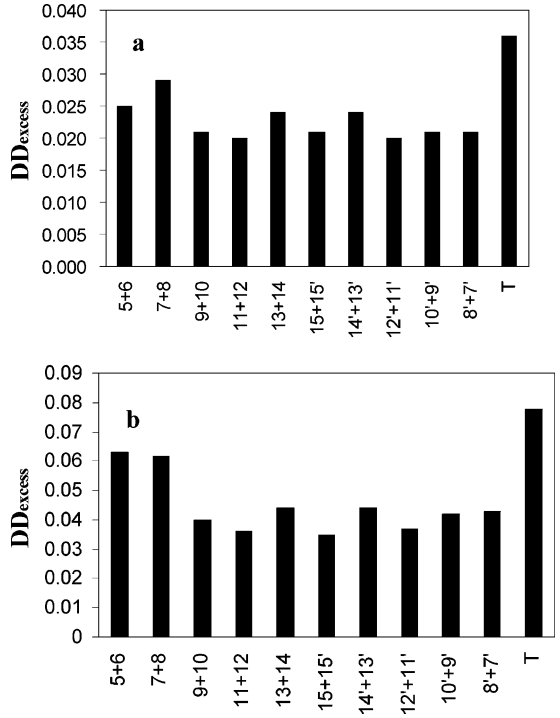

Figure 2. Calculated excess charge difference (DD_{excess}) between (a) $AMC^{\bullet+}$ and AMC, (b) between AMC^{2+} and AMC. The *y*-axis scale in b is twice that of a.

one around C5 and C6 and the other at T. Thus, stabilization of the dication by solvent as shown previously for β-carotene[1] has caused the oxidation potential to be similar to that of the radical cation using a carbon electrode.

The reduction CVs of AMC were also carried out with the gold and glassy carbon electrodes (Figure 3a). When the scan range is from 0 to −1600 mV, no reduction peak of AMC on the glassy carbon electrode was observed; however, a reduction peak (inset of Figure 3a) at −1185 mV for AMC on the chemisorbed gold electrode was detected, and no reverse oxidation peak was observed. Studies[8] show that SAMs on a gold surface are easily desorbed upon reduction between −0.7 and −1.1 V depending on the thiol derivative. Thus, the peak at −1185 mV is attributed to apparent reductive desorption,[8] that is, rupture of the C−S bond leaving S on the gold surface (ref 37). When the scan range is from −1400 to −2000 mV, a reduction peak was detected with each electrode; no reverse oxidation peak was observed in either case.

According to a previous study,[1] carotenoids that are not chemisorbed can also add two electrons. Because in the reduction of AMC, only one broad band is observed with the glassy carbon electrode, either only one electron is transferred, or the first and second reduction peaks overlap. The latter proved to be the case for the glassy-carbon electrode: high-resolution OSWV (Figure 3b) showed two peaks separated by only 66 mV. B3LYP/6-31G(d,p) calculations show that in $AMC^{\bullet-}$ the excess negative charge is distributed throughout the whole molecule (Figure 4a), and that in AMC^{2-} (Figure 4b) the excess negative charge (DD_{excess}) is localized around C7 and C8 and around C7′ and C8′. Note, the *y*-axis scale in Figure 4b is twice that of Figure 4a. No reverse oxidation peaks were detected in the CVs because $AMC^{\bullet-}$ and AMC^{2-} are either unstable or very reactive. The first and second reduction potentials on the gold and glassy carbon electrode determined by OSWV are listed in Table 1. The broad peak at −1.8 V is due to overlap of the first and second reduction peaks shifted to a more negative potential than on the glassy carbon due to modification of the

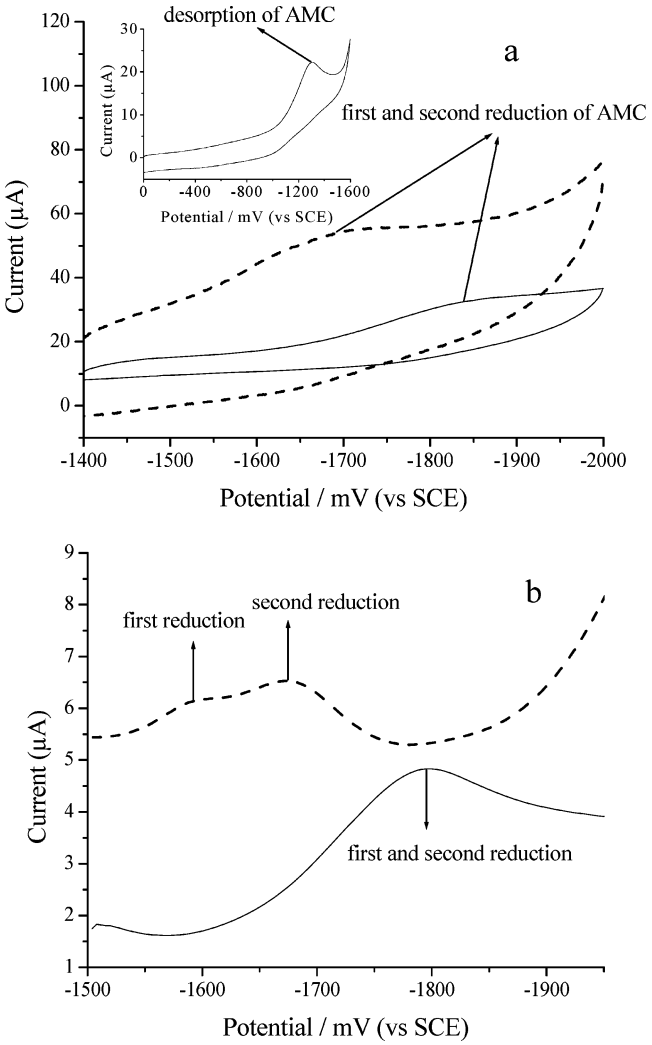

Figure 3. (a) Reduction−oxidation CV of AMC on a gold electrode (solid line) and a glassy carbon electrode (dashed line), scan range: −1400 to −2000 mV, scan rate: 1000 mV/s. Inset: reduction−oxidation CV of AMC on a gold electrode, scan range: 0 to −1600 mV, scan rate: 1000 mV/s. (b) OSWV for reduction of AMC on a gold electrode (solid line) and a glassy carbon electrode (dashed line) from −1500 to −1950mV.

gold electrode by the presence of S. This is noteworthy because now the first reduction potential on the gold electrode at −1.8 V is much lower than that on the glassy carbon electrode (by about 190 mV).

The hybrid density functional theory (DFT) method B3LYP[23] was used to study HOMO and LUMO energies of AMC, AMC−Au, AMC−Ag, and AMC−Cu. The basis set LanL2DZ[35,36] was used for all atoms in the geometry optimization without symmetry constraints. For thiolates chemisorbed on transition-metal surfaces, the metal cluster size affects the molecular orbitals' (MOs) eigenstates,[37] and the complex AMC−$(M)_n$ (M represents a metal, n is the number of metal atoms) were also calculated. Because AMC contains about 100 atoms, the calculation effort of AMC−$(M)_n$ would be huge. Fortunately, according to ref 37, only several MOs eigenstates exhibit a strong dependence on the size of the metal cluster, and other MOs change only slightly upon variation of the number of metal atoms. For thiolates chemisorbed on the Cu cluster,[37] only two MOs, both composed of C(2pz), S(3pz), and Cu(3d) contributions with energies around −9 eV, exhibit a strong dependence on the size of the Cu cluster.[37] The calculated HOMO and LUMO energies (see below) of AMC−Cu are much

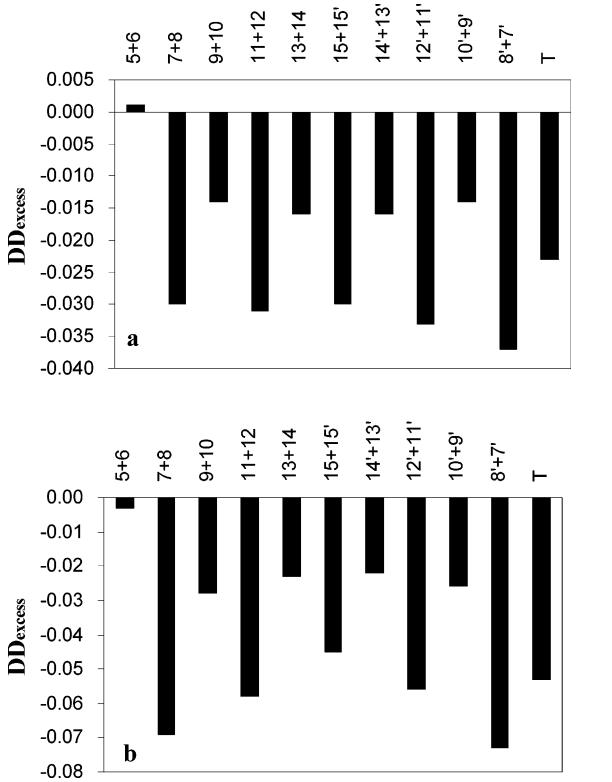

Figure 4. (a) Calculated excess charge difference (DD_{excess}) between $AMC^{\bullet-}$ and AMC, and (b) AMC^{2-} and AMC. The y-axis scale in b is twice that of a.

TABLE 2: Calculated HOMO and LUMO Energies (eV) for AMC, AMC−Au, AMC−Ag, and AMC−Cu

	AMC	AMC−Au	AMC−Ag	AMC−Cu
HOMO	−4.52	−4.50	−4.46	−4.46
LUMO	−2.42	−3.40	−2.99	−2.78

higher than −9 eV and thus can be considered to be approximately independent of the size of the metal cluster. The optimized geometries of AMC, AMC−Au, AMC−Ag, and AMC−Cu by B3LYP/LanL2DZ showed that the structure of AMC does not change significantly after the thiol H atom is replaced by the metal atoms. The respective C−C, C═C, C−H, and C−S bond lengths are very similar in the four structures. The bond lengths for S−Au, S−Ag, S−Cu, and S−H are 2.388, 2.438, 2.207, and 1.383 Å, respectively. Because the atom size decreases from Au to Ag to Cu to H, those bond lengths should decrease from S−Au to S−Ag to S−Cu to S−H. However, the calculations show that the bond length of S−Au is shorter than that of S−Ag, indicating that the bonding between S and Au in AMC−Au is stronger than that between S and Ag in AMC−Ag. The calculated HOMO energies, listed in Table 2, show that the HOMO energies of AMC−Au, AMC−Ag, and AMC−Cu are higher than that of AMC by 0.02, 0.06, 0.06 eV, respectively. The differences indicate that replacement of H with Au, Ag, or Cu causes a small change in the HOMO energy. The calculated LUMO energies, listed in Table 2, show that the LUMO energies of AMC−M are lower than that of AMC by 0.98, 0.57, and 0.36 eV for AMC−Au, AMC−Ag, and AMC−Cu, respectively, indicating that metal atoms cause the LUMO energy of AMC−M to be lower than that of AMC and the larger metal atom affects the LUMO energy more significantly than the smaller one. The DFT calculated ionization potential for AMC−Au is 121.9373 kcal/mol for oxidation and −50.1635 kcal/mol for reduction. For AMC, the DFT calculated

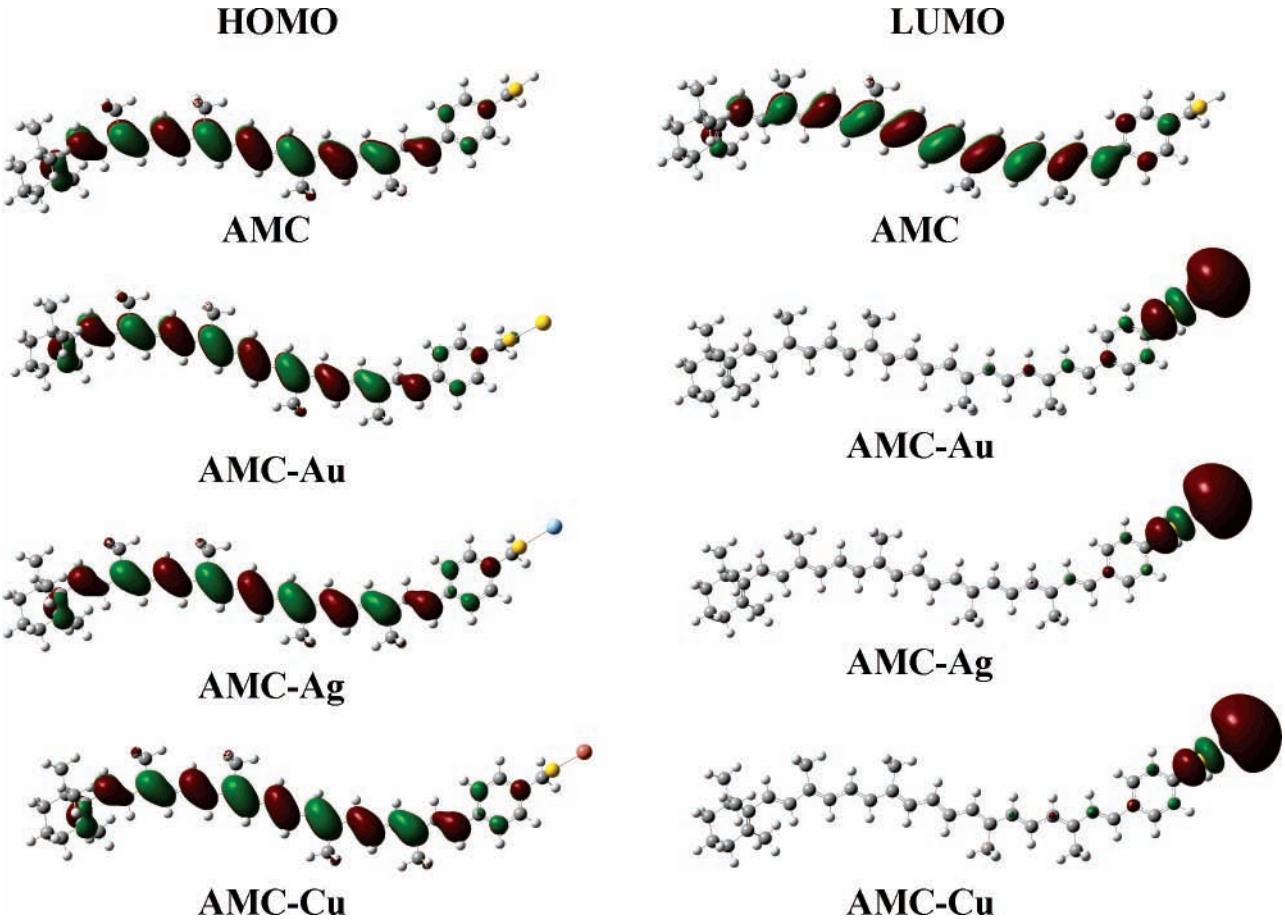

Figure 5. Calculated HOMO and LUMO surfaces of AMC, AMC−Au, AMC−Ag, and AMC−Cu. Green, positive wave function; red, negative wave function. H, light gray; C, dark gray; S, yellow (small); Au, yellow (large); Ag, light blue; Cu, brownish red.

ionization potential is 122.1602 kcal for oxidation and −39.9449 kcal/mol for reduction. The calculations are in agreement with the experimental data, which showed that the first oxidation potential of AMC−Au is lower than that of AMC. The first reduction potential for AMC−Au is predicted to be less negative than that for AMC. Unfortunately, reductive desorption by rupture of a C−S bond occurred before a reductive potential could be measured for AMC−Au. To understand these phenomena, the HOMO and LUMO surfaces of AMC, AMC−Au, AMC−Ag, and AMC−Cu were calculated and are shown in Figure 5. For the HOMO surfaces, the π orbitals are distributed over the whole conjugated system and there are no contributions from the atomic orbitals of the metals, which explains why the HOMO orbital energies are not affected by the metal atoms. However, for the LUMOs of AMC−M, the atomic orbitals of the metal (2s, 3s, and $5P_x$) and S ($3P_x$ and $4P_x$) make the largest contributions while those from C and H are very small, which explains why the metal atoms affect the LUMO energies significantly and why different metal atoms affect the LUMO energies of AMC−M differently.

To predict whether the above properties depend on the chain lengths of carotenoids, thiol-substituted carotenoids with different chain lengths were examined by B3LYP calculation. Chart 2 shows that **I** and **II** contain 2 and 4 fewer double bonds than AMC, respectively, and **III** contains 2 more double bonds than AMC. The HOMO and LUMO surfaces (Figure 6) of **I**−Au, **II**−Au, and **III**−Au by B3LYP/ LanL2DZ show that Au does not contribute to the HOMOs of those carotenoid−Au complexes and that Au and S make the largest contribution to the LUMOs of those complexes, which is just like AMC−transition

CHART 2

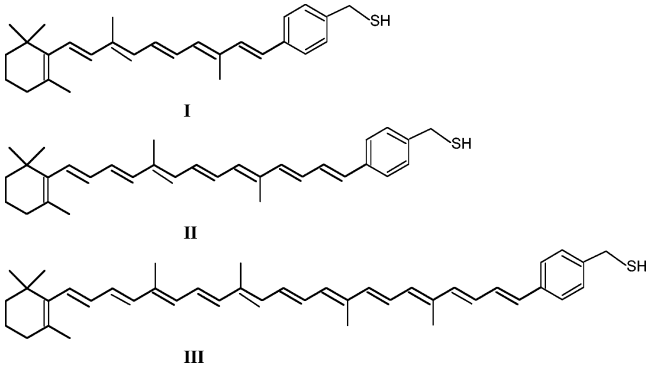

metal complexes, indicating that those properties are independent of chain lengths of carotenoids. The calculated HOMO and LUMO energies of **I**−Au, **II**−Au, **III**−Au, and AMC−Au listed in Table 3 show that the HOMO energies of those complexes increase with increasing chain length of carotenoid; however, the LUMO energies are the same for all of the species because the LUMOs consist of only S and Au atomic orbitals.

Conclusions

The dications of AMC are more stabilized than the radical ions because the two charges are localized at the two ends of the conjugated chain at a large distance from one another; the charge in the radical ion of AMC is delocalized throughout the whole conjugated system. These properties cause the similarity of the two oxidation potentials and the two reduction potentials

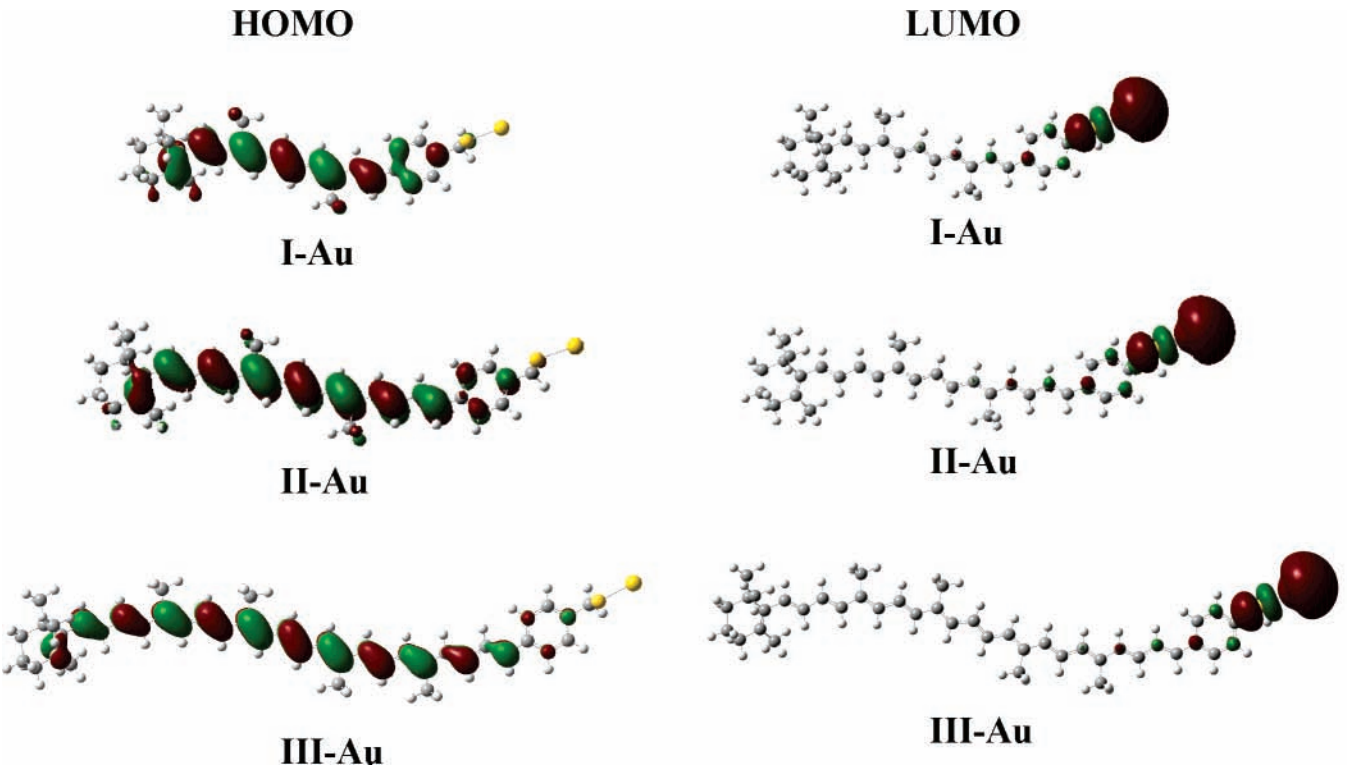

Figure 6. Calculated HOMO and LUMO surfaces of **I**−Au, **II**−Au, and **III**−Au. The color descriptions are the same as those of Figure 5.

TABLE 3: Calculated HOMO and LUMO Energies (eV) for I−Au, II−Au, AMC−Au, and III−Au.

	I−Au	**II**−Au	AMC−Au	**III**−Au
HOMO	−4.82	−4.68	−4.50	−4.49
LUMO	−3.40	−3.40	−3.40	−3.40

of AMC on a glassy carbon electrode. However, the solvation effect is suppressed when AMC is chemisorbed on the gold electrode. Chemisorbed AMC is reductively cleaved (C−S scission), at 1.185 V, leaving S attached to the Au electrode.

Bonding of AMC to the gold electrode facilitates the first electron transfer from AMC to the electrode. DFT calculations show that the LUMO orbital of AMC−M is composed of the atomic orbitals of S and the metal atoms and contribution from C and H atoms are small. Metal atoms cause the LUMO energy of AMC−M to be lower than that of AMC, and this effect is more significant for large metal atoms such as Au. Because the HOMO orbitals of AMC and AMC−M are distributed over the whole conjugated system and there is no contribution from the metal atom, the HOMO energies are not affected by metal atoms. Unfortunately C−S bond scission occurs before reduction can occur, leaving an S covered electrode remaining. DFT calculations also show that the HOMO energy of the carotenoid−transition metal increases with increasing chain length of the carotenoid and is independent of the transition metal. The LUMO energy of the complex does not depend on the chain length of the carotenoids but is affected by the transition metal.

Acknowledgment. We thank Dr. E. Hand for helpful discussions and Devens Gust for the sample of AMC. This work was supported by the Chemical Sciences, Geosciences and Biosciences Division, Office of Basic Energy Sciences, Office of Energy Research of the U.S. Department of Energy under Grant No. DE-FG02-86ER13465, by the start-up funds from Nanjing University (China) under Grant No. 0205005139, and by research funding from the Education Ministry of China under Grant No. 0205133142.

References and Notes

(1) Hapiot, P.; Kispert, L. D.; Konovalov, V. V.; Savéant, J.-M. *J. Am. Chem. Soc.* **2001**, *123*, 6669.

(2) Leatherman, G.; Durantini, E. N.; Gust, D.; Moore, T. A.; Moore, A. L.; Stone, S.; Zhou, Z.; Rez, P.; Liu, Y. Z.; Lindsay, S. M. *J. Phys. Chem. B* **1999**, *103*, 4006.

(3) Ulman, A. *Chem. Rev.* **1996**, *96*, 1533−1554.

(4) Love, J. Ch.; Estroff, L. A.; Kriebel, J. K.; Nuzzo, R. G.; Whitesides, G. M. *Chem. Rev.* **2006**, *10*, 1103−1169.

(5) Schreiber, F. *J. Phys.: Condens. Matter* **2004**, *16*, R881−R900.

(6) Schreiber, F. *Prog. Surf. Sci.* **2000**, *65*, 151−256.

(7) Gooding, J. J.; Mearns, F.; Yang, W.; Lui, *J. Electroanal.* **2003**, *15*, 81−96.

(8) Mirsky, V. M. *Trends Anal. Chem.* **2002**, *21*, 439−450.

(9) *Molecular Electronics*; Jortner, J., Rattner, M., Eds.; Blackwell Science: Malden, MA, 1997.

(10) Kunitake, M.; Akiyoshi, K.; Kawatana, K.; Nakashima, N.; Manabe, O. *J. Electroanal. Chem.* **1990**, *292*, 277.

(11) Bumm, L. A.; Arnold, J. J.; Cygan, M. T.; Dunbar, T. D.; Burgin, T. P.; Jones, L., II; Allara, D. L.; Tour, J. M.; Weiss, P. S. *Science* **1996**, *271*, 1705.

(12) Ulman, F. A. *Acc. Chem. Res.* **2001**, *34*, 855−863.

(13) Tour, J. M. *Acc. Chem. Res.* **2000**, *33*, 791−804.

(14) Chen, J.; Reed, M. A.; Rawlett, M. A.; Tour, J. M. *Science* **1999**, *286*, 1550−1552.

(15) Collier, C. J.; Wong, E. W.; Belohradsky, M.; Raymo, F. M.; Stoddart, J. F.; Kuekes, P. J.; Williams, R. S.; Heath, J. R. *Science* **1999**, *285*, 391−394.

(16) Liang, W.; Shores, M. P.; Bockrath, M.; Long, J. R.; Park, H. *Nature* **2002**, *417*, 725−728.

(17) Park, J.; Pasupathy, A. N.; Goldsmith, J. I.; Chang, C.; Yaish, Y.; Petta, J. R.; Rinkoski, M.; Sethna, J. P.; Abruna, H. D.; McEuen, P. L.; Ralph, D. C. *Nature* **2002**, *417*, 722−725.

(18) Selzer, Y.; Salomon, A.; Cahen, D. *J. Am. Chem. Soc.* **2002**, *124*, 2886−2887.

(19) Cui, X. D.; Primak, A.; Zarate, X.; Tomfohr, J.; Sankey, O. F.; Moore, A. L.; Moore, T. A.; Gust, D.; G. H.; Lindsay, S. M. *Science* **2001**, *294*, 571−574.

(20) Cui, X. D.; Zarate, X.; Tomfohr, J.; Primak, A.; Moore, A. L.; Moore, T. A.; Gust, D.; Harris, G.; Sankey, O. F.; Lindsay, S. M. *Nanotechnology* **2002**, *13*, 5−14.

(21) Liu, D.; Szulczewski, G. J.; Kispert, L. D.; Primak, A.; Moore, T. A.; Moore, A. L.; Gust, D. *J. Phys. Chem. B* **2002**, *106*, 2933.

(22) Rudolph, M.; Reddy, D. P.; Feldberg, S. W. *Anal. Chem.* **1994**, *66*, 589A.

(23) (a) Becke, A. D. *Phys. Rev.* **1988**, *A38*, 3098, (b) Becke, A. D. *J. Chem. Phys.* **1993**, *98*, 1372. (c) Becke, A. D. *J. Chem. Phys.* **1993**, *98*, 5648.

(24) Frisch, M. J.; Trucks, G. W.; Schlegel, H. B.; Scuseria, G. E.; Robb, M. A.; Cheeseman, J. R.; Montgomery, J. A., Jr.; Vreven, T.; Kudin, K. N.; Burant, J. C.; Millam, J. M.; Iyengar, S. S.; Tomasi, J.; Barone, V.; Mennucci, B.; Cossi, M.; Scalmani, G.; Rega, N.; Petersson, G. A.; Nakatsuji, H.; Hada, M.; Ehara, M.; Toyota, K.; Fukuda, R.; Hasegawa, J.; Ishida, M.; Nakajima, T.; Honda, Y.; Kitao, O.; Nakai, H.; Klene, M.; Li, X.; Knox, J. E.; Hratchian, H. P.; Cross, J. B.; Bakken, V.; Adamo, C.; Jaramillo, J.; Gomperts, R.; Stratmann, R. E.; Yazyev, O.; Austin, A. J.; Cammi, R.; Pomelli, C.; Ochterski, J. W.; Ayala, P. Y.; Morokuma, K.; Voth, G. A.; Salvador, P.; Dannenberg, J. J.; Zakrzewski, V. G.; Dapprich, S.; Daniels, A. D.; Strain, M. C.; Farkas, O.; Malick, D. K.; Rabuck, A. D.; Raghavachari, K.; Foresman, J. B.; Ortiz, J. V.; Cui, Q.; Baboul, A. G.; Clifford, S.; Cioslowski, J.; Stefanov, B. B.; Liu, G.; Liashenko, A.; Piskorz, P.; Komaromi, I.; Martin, R. L.; Fox, D. J.; Keith, T.; Al-Laham, M. A.; Peng, C. Y.; Nanayakkara, A.; Challacombe, M.; Gill, P. M. W.; Johnson, B.; Chen, W.; Wong, M. W.; Gonzalez, C.; Pople, J. A. *Gaussian 03*, revision C.02; Gaussian, Inc.: Wallingford, CT, 2004.

(25) Mairanovsky, V. G.; Engovatov, A. A.; Ioffe, N. T.; Samokhvalov, G. I. *J. Electroanal. Chem.* **1975**, *66*, 123.

(26) Khaled, M.; Hadjipetrou, A.; Kispert, L. D.; Allendoerfer, R. D. *J. Phys. Chem.* **1991**, *95*, 2438.

(27) Jeevarajan, A. S.; Khaled, M.; Kispert, L. D. *J. Phys. Chem.* **1994**, *98*, 7777.

(28) Chen, X., M. S. Thesis, University of Alabama, Tuscaloosa, 1991.

(29) Khaled, M., Ph.D. Dissertation, University of Alabama, Tuscaloosa, 1992.

(30) Jeevarajan, J. A.; Kispert, L. D. *J. Electroanal. Chem.* **1996**, *411*, 57.

(31) Jeevarajan, J. A.; Jeevarajan, A. S.; Kispert, L. D. *J. Chem. Soc., Faraday Trans.* **1996**, *92*, 1757.

(32) Jeevarajan, J. A., Ph.D. Dissertation, University of Alabama, Tuscaloosa, 1995.

(33) Liu, D.; Gao, Y.; Kispert, L. D. *J. Electroanal. Chem.* **2000**, *488*, 140.

(34) Hashimoto, H.; Yoda, T.; Kobayashi, T.; Young, A. J. *J. Mol. Struct.* **2002**, *604*, 125.

(35) Dunning, T. H., Jr.; Hay, P. J. In *Modern Theoretical Chemistry*; Schaefer, H. F., III, Ed.; Plenum: New York, 1976; Vol. 3, p 1.

(36) (a) Wadt, W. R.; Hay, P. J. *J. Chem. Phys.* **1985**, *82*, 284. (b) Hay, P. J.; Wadt, W. R. *J. Chem. Phys.* **1985**, *82*, 299.

(37) Konôpka, M.; Rousseau, R.; Stich, I.; Marx, D. *J. Am. Chem. Soc.* **2004**, *126*, 12103.